nature physics

SUPPLEMENTARY INFORMATION

https://doi.org/10.1038/s41567-018-0365-8

In the format provided by the authors and unedited.

Collective energy gap of preformed Cooper pairs in disordered superconductors

Thomas Dubouchet[1], Benjamin Sacépé[2]*, Johanna Seidemann[2], Dan Shahar[3], Marc Sanquer[1] and Claude Chapelier[1]*

[1]Univ. Grenoble Alpes, CEA, INAC, PHELIQS, Grenoble, France. [2]Univ. Grenoble Alpes, CNRS, Grenoble INP, Institut Néel, Grenoble, France. [3]Department of Condensed Matter Physics, Weizmann Institute of Science, Rehovot, Israel. *e-mail: benjamin.sacepe@neel.cnrs.fr; claude.chapelier@cea.fr

Supplementary Information of
Collective energy gap of preformed Cooper-pairs in disordered superconductors

Thomas Dubouchet,[1] Benjamin Sacépé,[2] Johanna Seidemann,[2]
Dan Shahar,[3] Marc Sanquer,[1] and Claude Chapelier[1]

[1] *Univ. Grenoble Alpes, CEA, INAC, PHELIQS, F-38000 Grenoble, France*

[2] *Univ. Grenoble Alpes, CNRS, Grenoble INP, Institut NEEL, F-38000 Grenoble, France*

[3] *Department of Condensed Matter Physics, Weizmann Institute of Science, Rehovot 76100, Israel*

I TRANSPORT MEASUREMENTS

In this section we present the transport properties of the four amorphous InO films studied in this work. Their respective thickness, superconducting critical temperature T_c and maximum sheet resistance above T_c are summarized in table S1. For a given thickness, the level of disorder is tuned by the partial oxygen pressure P_{O_2} used during the In_2O_3 evaporation.

Label	T_c (K)	$R_{\square}^{max}(\Omega)$	d (Å)
InO-1	1.45	5770	300
InO-2	1.5	5615	300
InO-3	1.9	3885	300
InO-4	3.2	400	700

TABLE S1: **Sample characteristics.** Critical temperature T_c, maximum sheet resistance $R_{\square}^{max}$ and sample thickness d of the four samples presented in Figure S1.

The T-evolutions of the sample resistances are shown in Figure S1. The critical temperature, T_c, is defined as the extrapolation to $R = 0$ of the resistance drop. T_c is in the range $1 - 2\,K$ for the three highly disordered films, InO-1, InO-2 and InO-3. This places them at the verge of the superconductor-insulator transition [1, 2]. The fourth film, InO-4, is much less disordered with T_c above $3\,K$ and behaves as a standard dirty BCS superconductor [3].

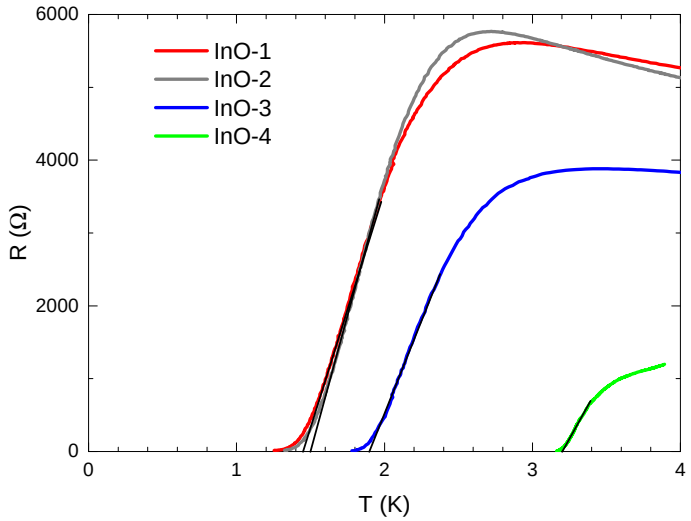

FIG. S1: **Superconducting transition of the indium oxide films.** T-evolutions of the resistance obtained during the cooling of the STM set-up. The black solid lines are linear extrapolations of the superconducting drop.

II EXTRACTION OF THE SPECTRAL GAP FROM TUNNELING SPECTRA

To estimate the spectral gap E_g of the one-particle density of states, we fit the low conductance point-contact data with BCS theory. Figure S2 shows a typical tunneling spectrum measured for a tunneling conductance of $0.42\,(2e^2/h)$, and a BCS fit (red curve) with $E_g = 650\,\mu eV$ and a Dynes parameter $\Gamma = 40\,\mu eV$ [4].

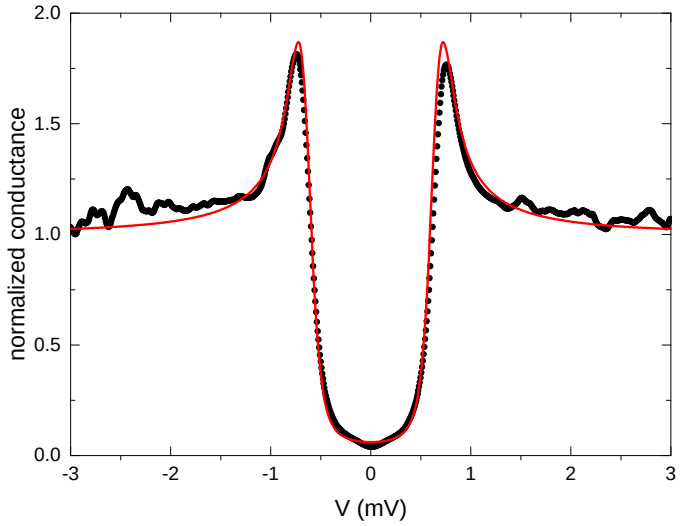

FIG. S2: **Tunneling density of states.** Spectrum measured with a tunneling conductance of $0.42\,(2e^2/h)$. The black dotted curve represents normalized experimental data. The red curve is a BCS fit.

III EVOLUTION FROM TUNNELING TO ANDREEV SPECTROSCOPY

Figure 1 of the main text shows an evolution from tunneling to point contact with a set of curves where the spectral gap E_g is much larger than the collective gap Δ_c. However, the spatial variation of E_g leads to situations where the difference between these two energy scales is significantly smaller. This is illustrated in Figure S3a-c that shows three other evolutions of the conductance acquired by approaching the STM tip toward the sample surface at three different positions. For each position, the spectral gap has been estimated by fitting with BCS theory a conductance curve measured in tunneling regime ($G(V) \ll 2e^2/h$) as shown in Figure S3d-f. For Figures S3d and S3f, the position of the coherence peaks in the $G(V)$ curves make the fit quite reliable despite the presence of a non-zero subgap conductance. This subgap conductance in Figure S2 was taken into account with the help of a phenomenological Dynes parameter with no impact in the estimation of E_g. However, close to the superconductor-insulator transition there is a substantial amount of spots where the spectral gap in the density of states is not bordered by coherence peaks on its edges. This already reported observation is the signature of the localization of Cooper-pairs in highly disordered superconductors [5]. An example is shown in Figure S3e. In such a situation, although the BCS fit leads to a less accurate estimation of E_g, the spectral gap can still be clearly distinguished from the collective gap. The latter is signaled by intra-gap Andreev peaks appearing in point contact regime ($G(V) \geq 2e^2/h$) as shown in the green curves of Figure S3d-f. While E_g is varying by more than a factor 3 in the four evolutions shown (Figure 1 and Figure S3), Δ_c remains in the range $145 \pm 30\,\mu$eV as reported in the main text.

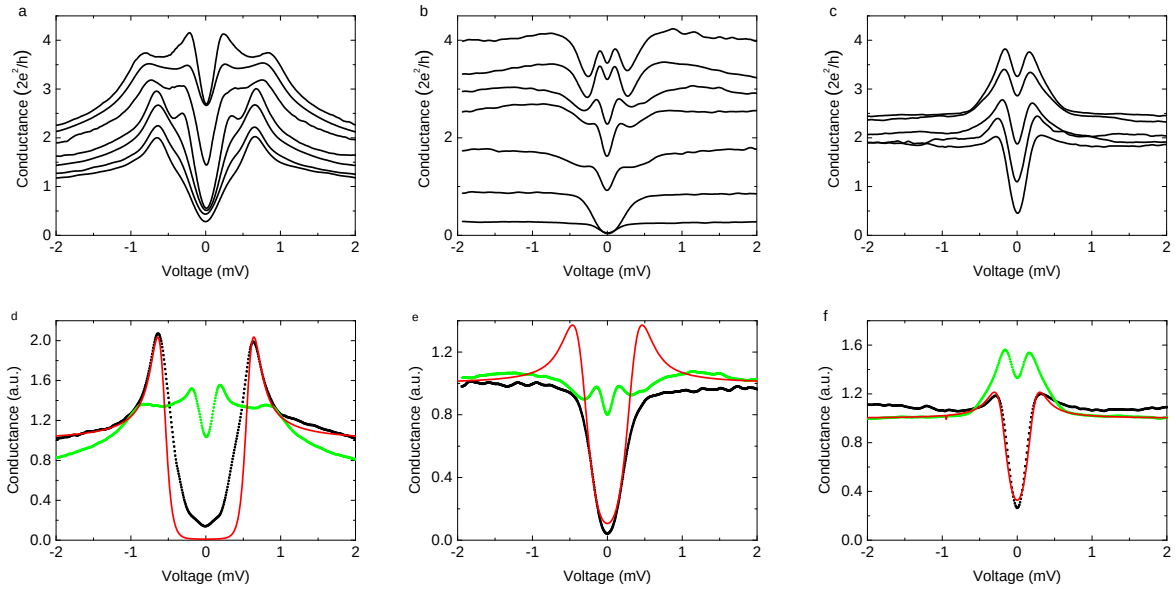

FIG. S3: **From tunneling to Andreev spectroscopy.** Panels in the same row correspond to data acquired at the same STM tip position. **a-c,** Evolutions of the local conductance $G(V)$ measured at $T = 0.065$ K by bringing into contact the STM tip and the sample surface on InO-2 (panel a) and at two different tip positions on InO-3 (panels b and c). The conductance is in units of $2e^2/h$ and has not been vertically shifted. **d-f,** Measurement of the two energy scales. E_g is estimated in tunneling regime (black curves) by fitting the BCS density-of-states (red curve). The Andreev peaks which emerge in point contact regime (green curves) give a measurement of Δ_c . **a**: $E_g = 580 \pm 20\,\mu$eV and $\Delta_c = 170 \pm 15\,\mu$eV. **b**: $E_g = 340 \pm 20\,\mu$eV and $\Delta_c = 130 \pm 20\,\mu$eV. **c**: $E_g = 200 \pm 20\,\mu$eV and $\Delta_c = 160 \pm 10\,\mu$eV.

IV ANDREEV SIGNAL STRENGTH

The point contact resistance between the STM tip and the sample could not be made arbitrarily low. This non-zero barrier height prevents the Andreev signal at the Fermi energy from reaching the doubling of the conductance measured at high voltage or in the normal state [6]. Moreover, due to the finite size of the contact, the total conductance comprises several channels characterized by different barrier heights Z. Whereas the transmission above the gap depends on Z^2, the Andreev reflexion below the gap depends on Z^4 [6]. The Andreev signal is therefore dominated by few transparent channels. On the other hand, the coherence peak height measured in tunneling regime is strongly fluctuating as already reported in ref. [5]. For these reasons, the ratio between the peak heights at E_g and Δ_c in point contact regime is varying quite significantly for different realizations. This is illustrated in Figure S4 where three spectra taken on different samples show different peak

heights ratios. In the left panel the peak at Δ_c is much weaker than the peak at E_g whereas both are comparable in the middle panel, for a similar contact conductance. On the right panel the peaks at $\pm E_g$ which was observed in tunneling regime (not shown) has been fully washed out by the very strong Andreev peaks. Note that in this case the conductance ($\sim 5.4\,(2e^2/h)$)is higher than for the two other spectra.

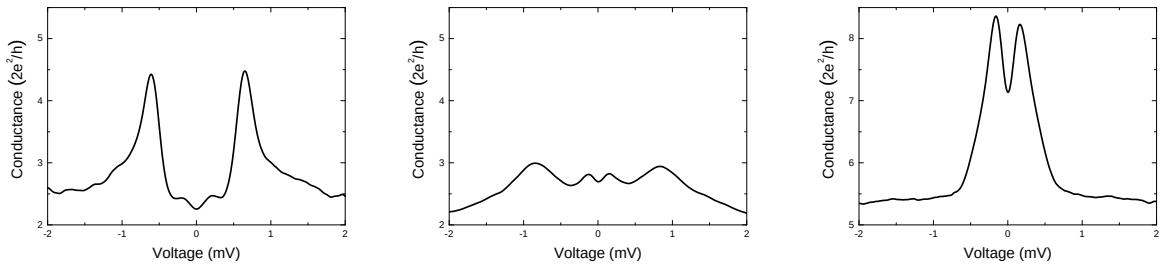

FIG. S4: **Andreev spectra.** Conductance $G(V)$ curves measured in point contact regime on samples InO-1, InO-2 and InO-3 from left to right.

V SECOND DERIVATIVE OF THE CONDUCTANCE

The collective gap (Δ_c) can be readily evaluated with the position of the Andreev peaks in point-contact spectra $G(V)$ acquired at high conductance such as the one shown in Figure 1 of the main text where these peaks are well defined. The energy of the Andreev peaks can also be determined by inspecting the second derivative $-d^2G/dV^2$ as illustrated in Figure 2 of the main text. This proves to be useful when the peaks at E_g and Δ_c nearly overlap and are difficult to resolve. An example is shown in the point-contact evolution of Figure S5. The Andreev peaks are signaled by a change of slope in the raw conductance (red vertical line in the left panel) which becomes more pronounced when the point-contact conductance increases. In the second derivative of the conductance, at this same energy a well-defined peak grows which enables a more accurate determination of Δ_c.

VI THERMAL EVOLUTION OF ANDREEV SPECTRA

In this section, we detail the analysis of the T-evolution of Andreev spectra. In Figure 2a of the main text a few selected $G(V,T)$ acquired on InO-2 are displayed. We show in Figure S6 the complete set of curves for this data acquisition taken between $T = 0.15$ K and $T = 1.6$ K, without

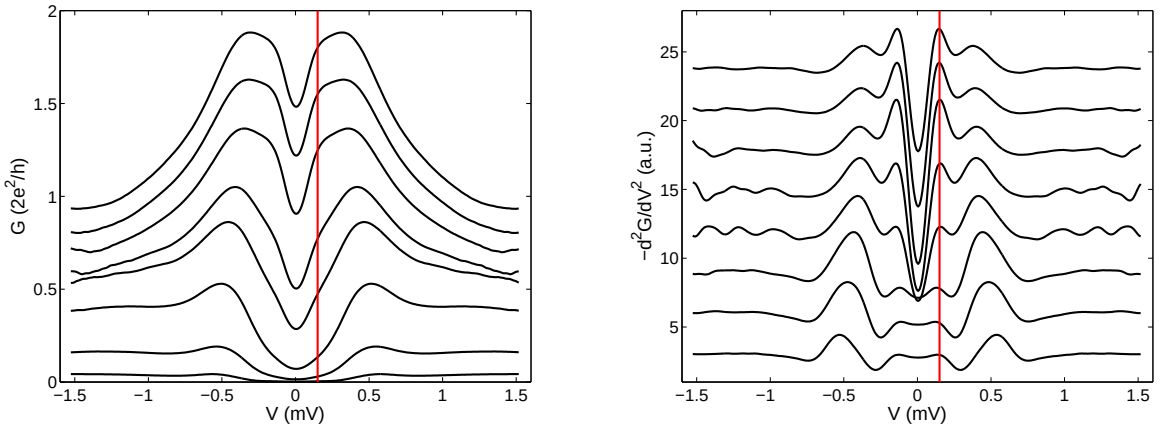

FIG. S5: **Second derivative of an Andreev spectrum.** Left : Evolution of the local conductance $G(V)$ for different values of the point-contact conductance acquired on sample InO-3. Right : second derivative $-d^2G/dV^2$ (arbitrary unit) of the same data. The vertical red lines, both at the same voltage bias, point out the position of the Andreev peak at Δ_c in both panels.

any vertical shift. The decrease of the conductance around $T_c = 1.5$ K (orange-red curves) reveals the appearance of the non-zero resistance state of the film. This can be evidenced by comparing the thermal evolution of the inverse of the conductance at the set-point bias ($1/G(-2mV, T)$) with the foot of the $R(T)$ superconducting transition in the vicinity of T_c, as shown in Figure S6b. We indeed see that both curves start to increase at the same temperature.

We show in Figures S7 and S8 another T-evolution of an Andreev spectrum measured on sample InO-3 between 0.165 K and 2.12 K. Spectra for selected temperatures are plotted in Figures S7a with a vertical shift for the sake of clarity and the whole set of conductance curve data is displayed in Figure S8a with no vertical shift. As shown in Figure S7b the increase of the inverse of the conductance measured at the set-point bias coincides with the increase of the resistance of the film near T_c (1.9 K) in a similar way as discussed above for InO-2.

For both thermal evolutions, slightly above the superconducting critical temperature the vanishing Andreev contribution is due to the existence of short-lived fluctuating Cooper pairs in the film. The computed second derivative $-d^2G/dV^2$ of the spectra displayed in Figure S8a has been plotted in Figure S8b. It leads to a better resolution of the Andreev peaks near T_c as illustrated in Figure S8c and S8d which display the same data but in a limited range of temperature near T_c. This allows to measure the closing of Δ_c with the increase of T as shown in Figure S9.

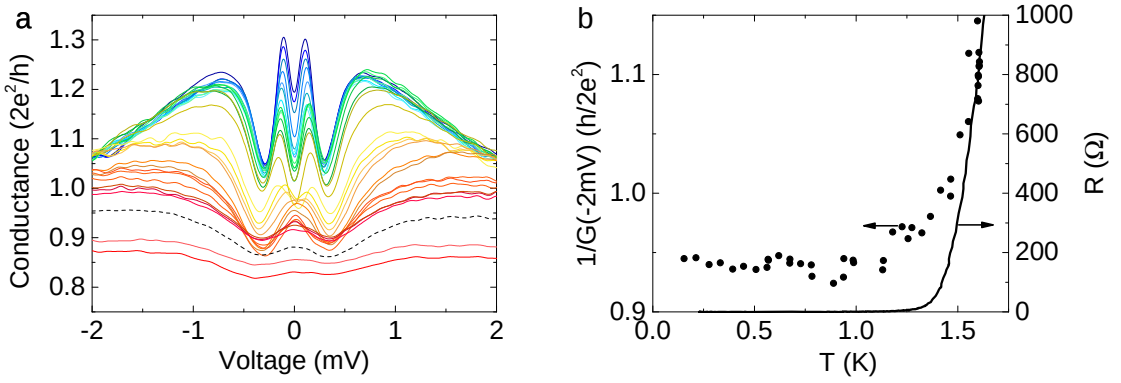

FIG. S6: **Temperature evolution of the Andreev spectrum of Figure 2b. a,** Local conductance curves $G(V)$ (without vertical shift) measured between $T = 0.15$ K (top curve) and $T = 1.6$ K (bottom curve) at the same location on sample InO-2. The dashed curve has been acquired at $T = T_c$. **b,** Comparison of the T-evolution near T_c of the inverse of the conductance at the set-point bias $(1/G(-2mV))$ and of the resistance of the film.

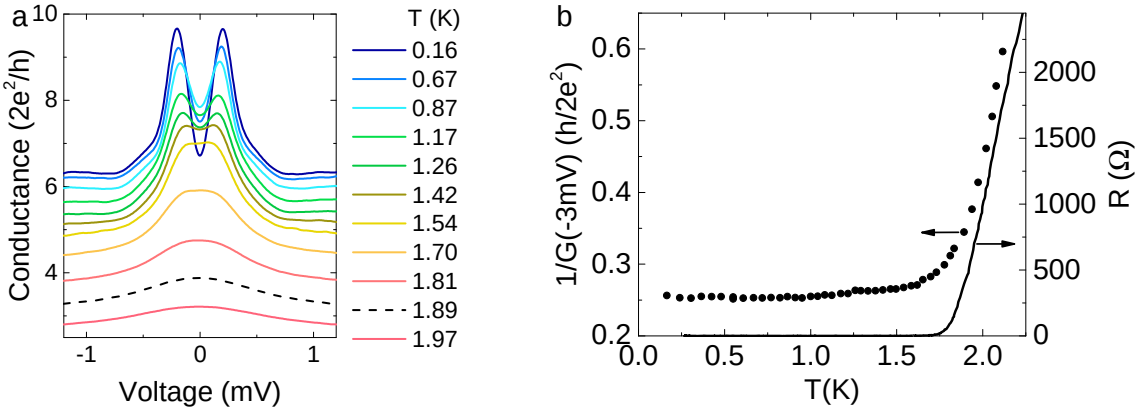

FIG. S7: **Temperature evolution of an Andreev spectrum measured on InO-3. a,** Local conductance curves $G(V)$ measured at the same position and different temperatures. All curves except the bottom one are vertically shifted for clarity. The shift between two consecutive curves is equal to $0.2\,(2e^2/h)$. The dashed curve has been acquired at T_c. **b,** Comparison of the T-evolution near T_c of the inverse of the conductance at the set-point bias $(1/G(-3mV))$ and of the resistance of the film InO-3.

VII T-EVOLUTION OF THE TUNNELING CONDUCTANCE

We present in this section the T-evolution of the tunneling density of states in a highly disordered sample (InO-2) and a low disordered sample (InO-4), see parameters in Table S1. Figure S10 displays the colormap of the tunneling conductance as a function of voltage bias and reduced temperature T/T_c. A clear pseudogap develops above T_c for the highly disordered sample (see

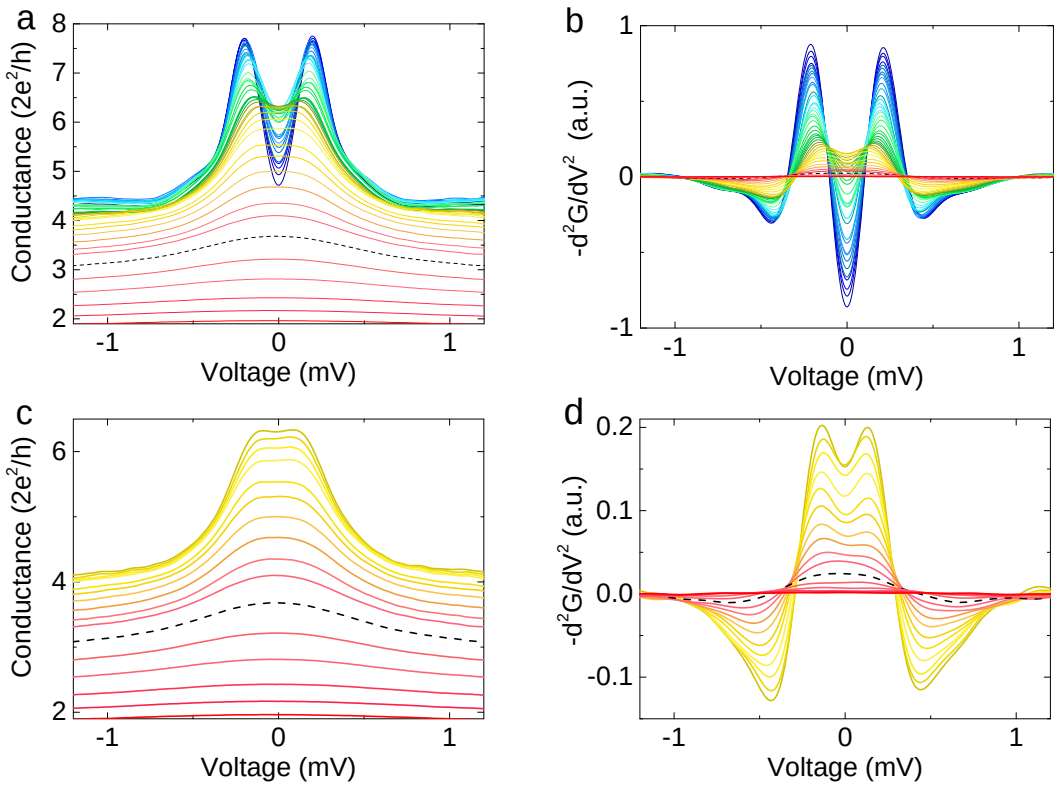

FIG. S8: **Detailed analysis of the temperature evolution of the Andreev spectra of Figure S7. a,** Conductance curves $G(V)$ measured between $T = 0.165$ K (top curve) and $T = 2.12$ K (bottom curve). The dashed curve has been acquired at T_c. **b,** Second derivative $-d^2G/dV^2$ (arbitrary unit) of the same data as in panel a. **c,** Selected $G(V)$ curves acquired in the vicinity of T_c between $T = 1.5$ K (top curve) and $T = 2.12$ K (bottom curve). **d,** Double derivation of the data of panel c.

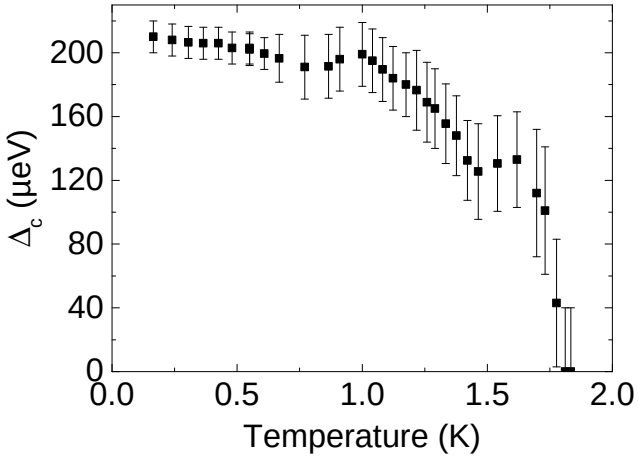

FIG. S9: **Temperature dependence of the collective evergy gap.** Δ_c versus T extracted from the data shown in Fig. S8.

Fig. S10a) together with a suppression of the coherence peaks near T_c, as reported in Ref. [5]. This is

the hallmark of the pseudogap state which reveals the presence of preformed Cooper pairs. The low disordered sample (InO-4) does not exhibit such a strong pseudogap. Instead, the superconducting gap is suppressed around $T \sim 1.2T_c$, see see Fig. S10b, signaling a small depression in the density-of-states above T_c due to superconducting fluctuations. A BCS fit (not shown) of the tunneling spectrum acquired at 50 mK gives a superconducting gap of 670 μeV, leading to a ratio $E_g/k_BT_c = 2.4$ much smaller than the typical one measured in the three highly disordered samples [5]. There is therefore neither preformed Cooper pairs nor strong pseudogap regime far above T_c in contrast with samples InO-1, InO-2 and InO-3 that are close to the superconductor-insulator transition [5].

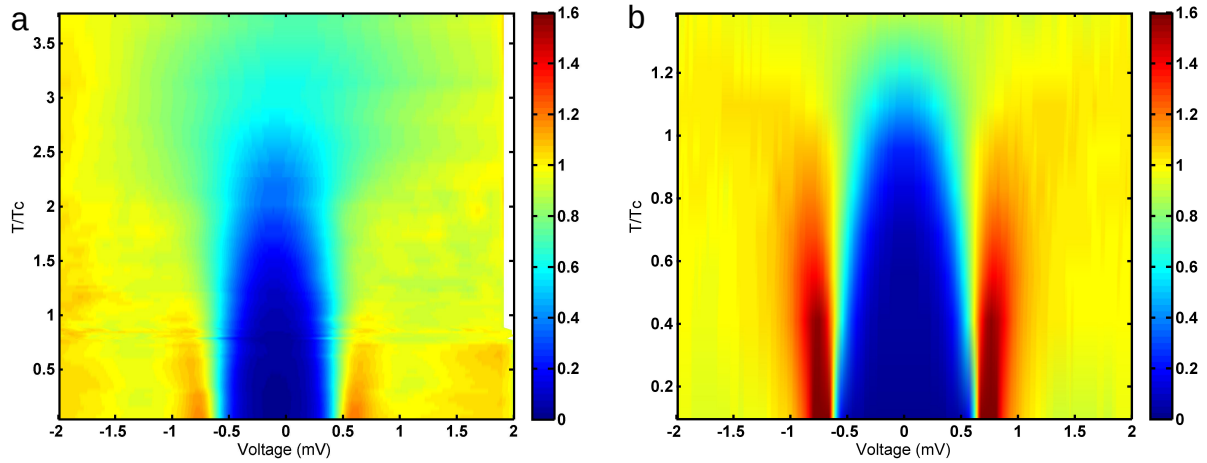

FIG. S10: **Pseudogaps.** Colormap of the normalized tunneling conductances versus voltage bias and reduced temperature, measured in the tunneling regime with $G(-3mV) = 0.001\, e^2/h$ for sample InO-2 in **a**, and with $G(-3mV) = 0.004\, e^2/h$) for sample InO-4 in **b**.

VIII ANDREEV SPECTROSCOPY OF THE LOW DISORDER SAMPLE

We performed Andreev spectroscopy on the low disorder sample InO-4. Figure S11 shows typical differential conductance curves from tunneling to Andreev regime. In the Andreev regime, the in-gap conductance increases continuously, without additional peaks. Those Andreev spectra can be accurately fitted with the Blonder-Tinkham-Klapwijk theory (BTK) [6] which enables to extract the barrier strength Z. This conventional behavior proves that far from the superconductor-insulator transition, a single energy scale controls the transition to the superconductor as expected in BCS theory.

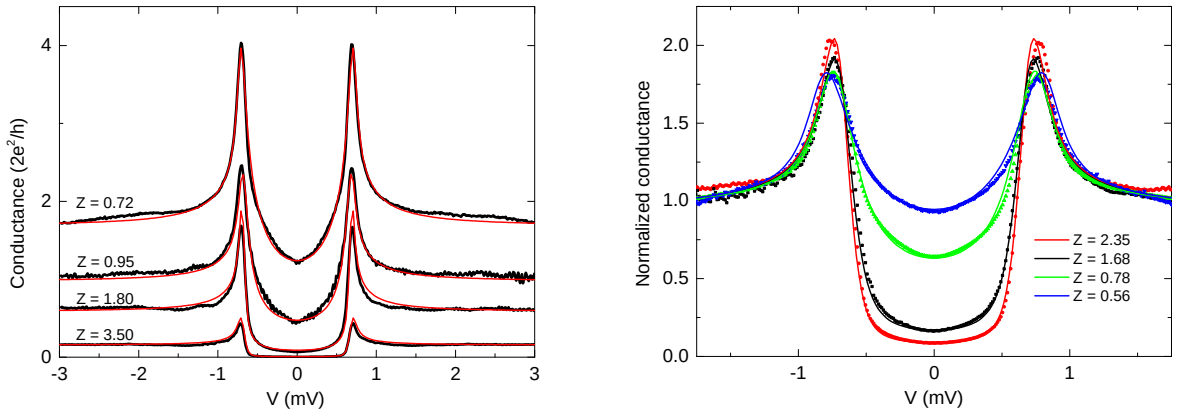

FIG. S11: **Andreev Spectroscopy of a low disordered a:InO film**. The dotted curves are experimental data and the lines are BTK fits with a fitting parameter Z which represents the tunneling barrier height. Left : the conductance has been expressed in unit of the quantum of conductance for a comparison with Figure 1 of the main text. Right : another set of data normalized at high bias.

[1] Shahar, D., Ovadyahu, Z. Superconductivity near the mobility edge. *Phys. Rev. B* **46**, 10917–10922 (1992).

[2] Gantmakher, V.F., Golubkov, M.V. Giant negative magnetoresistance of semi-insulating amorphous indium oxide films in strong magnetic fields. *Sov. Phys. JETP* **82**, 951 (1996).

[3] Sacépé, B.,*et al.* High-field termination of a Cooper-pair insulator , *Phys. Rev. B* **91**, 220508(R) (2015).

[4] White, E., Dynes, R.C., and Garno, J.P. Destruction of superconductivity in quench-condensed two-dimensional films. *Phys. Rev. B* **33**, (R)3549–3552 (1986).

[5] Sacépé, B., Dubouchet, T., Chapelier, C., Sanquer, M., Ovadia, M., Shahar, D., Feigel'man M. & Ioffe, L. Localization of preformed Cooper pairs in disordered superconductors. *Nature Phys.* **7**, 239–244 (2011).

[6] Blonder, G.E., Tinkham, M. & Klapwijk, T.M. Transition from metallic to tunneling regimes in superconducting microconstrictions: Excess current, charge imbalance, and supercurrent conversion. *Phys. Rev. B* **25**, 4515–4532 (1982).